Cycling performance of the Li_xAl anode prepared by the compression method

R.V. Moshtev[a], P. Zlatilova[a], B. Puresheva[a], V. Manev[a] and A. Kozawa[b]
[a]*Central Laboratory of Electrochemical Power Sources, Bulgarian Academy of Sciences, Sofia 1113 (Bulgaria)*
[b]*Chubu University, Kasugai, Aichi 487 (Japan)*

(Received August 17, 1993; in revised form January 27, 1994; accepted January 29, 1994)

Abstract

A preparation method of Li–Al anodes by compression of foils of the two metals at room and elevated temperatures is described. The chemical diffusion coefficient of lithium in the Li–Al anodes is measured as a function of the lithium concentration in the β-phase range. The cycleability of the anodes prepared by this method with and without manganese is studied in laboratory coin cells, with L_xMnO_2 cathodes, as a function of the depth-of-discharge (DOD). The cycling efficiency of the Mn-free anodes at DOD = 22% is very low, 88.9%, while that of the anodes with 1.0 and 2.6% Mn is considerably higher: 95.5% at DOD 17% and 94.4% at DOD 38%, respectively.

Introduction

Unsatisfactory cycleability and safety problems inherent to the rechargeable lithium anode have inspired wide investigations aimed at finding radical means to overcome these drawbacks. One of the approaches, which has reached a commercial development, is the replacement of the pure Li with lithium alloys and more specifically with the Li–Al alloy [1]. The major part of the previous research work was dedicated to the task to determine the optimum conditions for the formation of high performance Li–Al anodes by Li electrodeposition on an Al substrate [2–7]. Fewer are the investigations of Li–Al anodes prepared by pressing of a powdered Li–Al alloy, obtained by pyrometallurgical techniques [5, 8, 9]. The third, more recent, method for the preparation of Li–Al anodes is the alloying by contacting foils of the two metals with or without pressure at room and elevated temperatures. This method is described in two patent specifications [10, 11].

The basic property which makes the β-phase a good rechargeable anode material for nonaqueous cells is its high Li-diffusion coefficient. For a successful cycling, high rate and high energy performance the Li–Al anode should possess some additional properties:

(i) a well-developed surface area and sufficient porosity securing a rapid exchange of Li at the liquid/solid interface;

(ii) a rigid crystal macrostructure composed of tightly bound crystal agglomerates, with a sufficient thickness, capable of delivering a large capacity per unit area;

(iii) rigid crystal grains with sufficient mechanical resistance against the propagation of cracks during cycling, and

0378-7753/94/$07.00
SSDI 0378-7753(94)01916-J

(iv) a strong and reliable bond between the β-Li–Al layer and the underlying Al substrate, serving as a mechanical reinforcement and a current collector.

Some of these properties are related to the porosity of the β-Li–Al layer. The high porosity, which is characteristic for the electrochemically formed Li–Al anodes, provides high rate capability but also a low mechanical resistance. Consequently, these anodes are with a lower cycling efficiency at higher depth-of-discharge (DOD) and with a smaller capacity per unit area due to their limited thickness. On the other hand, the anodes prepared by pressing of powdered Li–Al alloy at 6 tons/cm^2 followed by sintering at ~350 °C in pure helium atmosphere [5] have a limited porosity, 35 to 45%, and an enhanced mechanical stability, whereby their thickness and, consequently, their capacity per unit surface area can be considerably increased. The method of preparation is, however, rather sensitive to atmospheric contaminations and their best performance characteristics are difficult to be reproduced.

It is the aim of this paper to investigate the method of preparation of Li–Al anodes based on the compression of the two metals at room and elevated temperatures and to study the performance of these anodes in secondary Li_xAl/Li_yMnO_2 button cells in a wide range of DOD. The effect of manganese content in the Li–Al anodes on its electrochemical characteristics was also studied.

Part 1. Preparation of the Li–Al anodes

Experimental

Three kinds of substrate were used in order to examine the effect of Mn on the preparation variables and on the cycling performance of the anodes:

(i) high purity Al (Al, 99.99%);

(ii) single-phase Al alloy with 1.0% Mn, and

(iii) two-phase Al alloy with 2.6% Mn.

The primary melts of pure Al with Mn were subjected to a fast quenching followed by a deep plastic deformation consisting of a two-stage 20-step cold rolling process to produce foils of the necessary thicknesses. As a result of these operations the pure Al foil showed only a substructural orientation without macrostructurally expressed grain boundaries. In the single-phase Al alloy with 1.0% Mn the latter is completely in the form of a solid solution. The plastic deformation of this alloy results in a slight reduction of the crystal grains. The two-phase Al–Mn alloy reveals clearly the grains of the second intermetallic phase, $MnAl_6$, which undergo a considerable disintegration during the plastic deformation, but their good cohesion with the Al matrix is preserved.

The Al foils were etched in a warm 3 N KOH solution and, after rinsing and drying, they were cut into discs of 15 mm in diameter. Lithium discs of the necessary thickness were prepressed to the Al discs in a die for several min at ~200 to 500 kg/cm^2 and then transferred in a jig, where they were subjected to a pressure of ~1.5 tons/cm^2 at room or elevated temperature. Preliminary experiments revealed that a comparatively good cycling performance is achieved with anodes containing an overall Li concentration of ~14 w/o. This concentration is obtained when the thickness ratio of the Al and Li discs is as 1.2:1. Since the Li concentration in the β-phase layer is ~20 w/o it is clear that, at this overall Li concentration, part of the Al foil remains unalloyed (~25% in thickness) and it serves as reliable current collector and a mechanical reinforcement base.

After being kept for a definite time under pressure in a jig (τ) the Li–Al couple was transferred to a three-electrode electrochemical cell with an electrolyte of 1 M

$LiClO_4$ in propylene carbonate–dimethoxyethane (PC–DME) (1:1) and the open-circuit potential versus Li/Li^+ reference electrode was measured after a short equilibration time. The measurement of the Li chemical diffusion coefficient, D, was performed in the same cell by the galvanostatic polarization method at two current densities ($i < 0.25$ mA/cm^2). The cathodic overpotential was followed during the first 900 s, where the condition $t \ll L^2/D$ is fulfilled and the expression:

$$D = \left[\frac{2V_m i(dE/dx)}{\sqrt{\pi}F(dE/d\sqrt{t})}\right]^2 \quad (1)$$

is valid. The charges applied in the D measurements were only ~1% of the excess capacity of the β-Li–Al anode so that the appearance of any new phase is excluded. The molar volume of β-Li–Al, V_m, was calculated with the average density of this phase in the composition range of 47 to 53 a/o, $d = 1.7$ g/cm^3 [12]. The value of $dE/dx = 0.415$ V/equiv. is that determined in ref. 5 with Li–Al alloys prepared by the pyrometallurgical method.

For the scanning electron microscope (SEM) pictures, the specimens were transferred from the dry box in a vacuum vessel to the vacuum chamber where they were coated with a 100 Å gold film, before being introduced into the electron microscope. The cross section was prepared by cutting the sample in the dry box with a thin rotating disc knife under a slight pressure in order to avoid any deformation of the structure.

Results and discussion

The evolution of the open-circuit potential, $E°$, with the time of alloying of the anodes is given in Fig. 1, where each experimental point corresponds to a new Li–Al couple obtained from Li and Al discs with a thickness of 125 and 150 μm, respectively.

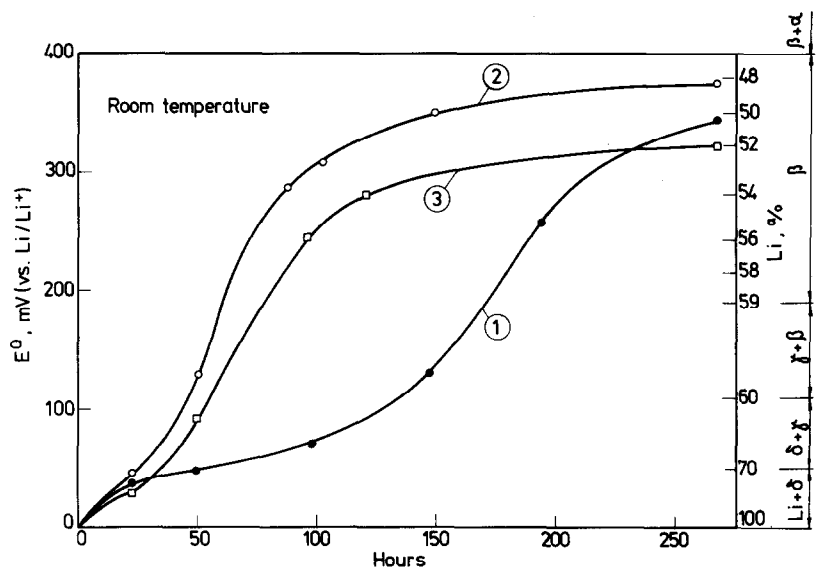

Fig. 1. Typical $E°$–τ curves of Li–Al couples during alloying at room temperature: (1) without applied pressure with Mn-free Al foil; (2) under ~1.5 tons/cm^2 with Mn-free Al foil, and (3) under ~1.5 tons/cm^2 with Al foil containing 2.6% Mn.

Figure 1 demonstrates three typical $E°$–τ curves obtained with Li–Al anodes alloyed at room temperature, where curve 1 corresponds to a Mn-free Al disc without external pressure, curve 2 to a Mn-free Al disc under ~1.5 tons/cm^2 and curve 3 to an Al disc containing 2.6% Mn under 1.5 tons/cm^2. The at.% Li concentration corresponding to the respective potential values is indicated on the right-hand ordinate on Fig. 1, together with the stability regions of the phases of the Li–Al system, as reported by Jow and Liang [5].

Curve 1 in Fig. 1 reveals four stages of the alloying reaction, corresponding to the phases prevailing on the anode surface observable more clearly at room temperature and without external pressure. The first stage extends to a plateau at ~50 mV, where the anode surface consists of metallic Li together with the Li-rich δ phase. When the metallic Li is exhausted and the 50 mV plateau is reached, the surface contains the δ and γ phases. It should be noted here that, despite the insignificant potential change of only 50 mV, the rate of the alloying reaction in these two stages is very high as exhibited by the decrease in the surface Li concentration from 100 to ~70 a/o. The next stage is marked by a steep rise of the potential with time and reflects the formation of the β phase, characterized by a strong dependence of $E°$ on the Li concentration. As the latter drops to below 50 a/o and the chemical potential difference at the reaction interface becomes very low, the reaction rate falls sharply and the potential tends to a saturated value.

Curve 2 in Fig. 1 illustrates the strong accelerating effect of pressure on the alloying reaction while curve 3 shows that the presence of Mn has a retarding effect.

Figure 2 demonstrates the simultaneous accelerating effect of P and t on the alloying process as well as the retarding effect of Mn. It is seen that, by increasing the temperature and pressure, the time of contact necessary to form the β-phase can be considerably reduced. It was found, however, that raising of the temperature above 70 °C and the pressure above 1.5 tons/cm^2 leads to an undesired increase in the

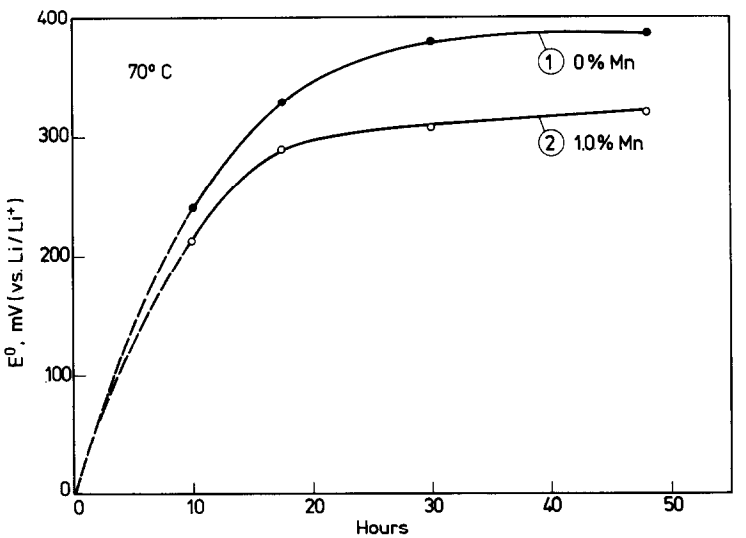

Fig. 2. Typical $E°$–τ curves of Li–Al couples during alloying at 70 °C and ~1.5 tons/cm^2: (1) with Mn-free Al foil, and (2) with Al foil containing 1.0% Mn.

plasticity of Li, whereby it is squeezed out of the Al foil, leading to an uncontrollable loss of Li. In this case it was impossible to prepare anodes with a definite composition.

The intermetallic reaction (Li + Al ⇒ β-Li–Al) is exothermal with an enthalpy of 0.38 eV. Assuming hypothetically a pore-free β-Li–Al layer it can be estimated that at the thickness ratio employed in our experiments (Li:Al = 1.2:1) the volume reduction after alloying will be ~11%. Hence, according to the principle of Le Chatelier–Braun, the application of an external pressure will tend to shift the equilibrium in the direction of the β-phase formation. The considerable increase in the reaction rate upon the application of pressure is in accordance with this principle.

It should be emphasized that the initially applied pressure in the jigs is not maintained entirely constant throughout the anode formation. Actually, the pressure is slightly decreasing with time on account of the volume contraction inherent to the alloying reaction. Since in fact the jigs secure a constant volume, the contraction will result in the formation of voids in the β-phase layer. This is demonstrated by the SEM picture of the cross section of the anode in Fig. 3 revealing the macrostructure of the layer with a porosity diminishing in the direction of the Al substrate. This pore distribution is to be assigned to the immobility of the Al atoms with respect to that of the Li atoms [12]. The last-named leave the initially formed Li-rich layers at the Li side of the Li–Al couple and are rapidly transferred into the Al phase, thus forming voids behind them.

The macro- and microstructure of the Li–Al anodes prepared by the present method with 0, 0.1 and 2.6% Mn is shown by SEM pictures in Figs. 4 and 5. At lower magnifications of ×100, one can see the comparatively even and homogeneous surface formed by the plates of the compression jigs. The stratified surface structure is visible in the ×1000 magnification pictures in Fig. 4 in all three samples. These

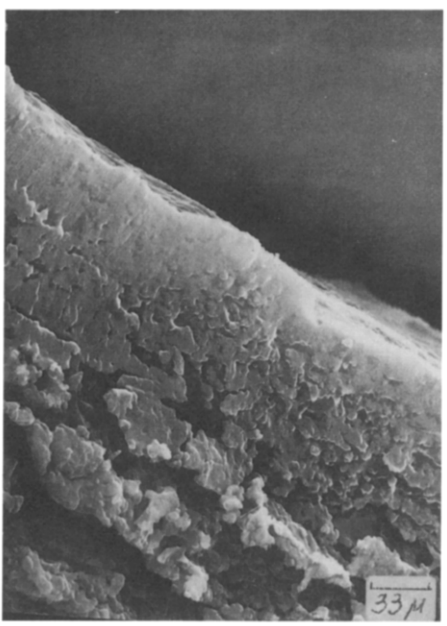

Fig. 3. SEM picture of the cross section of an Li–Al electrode with 1.0% Mn; ×300.

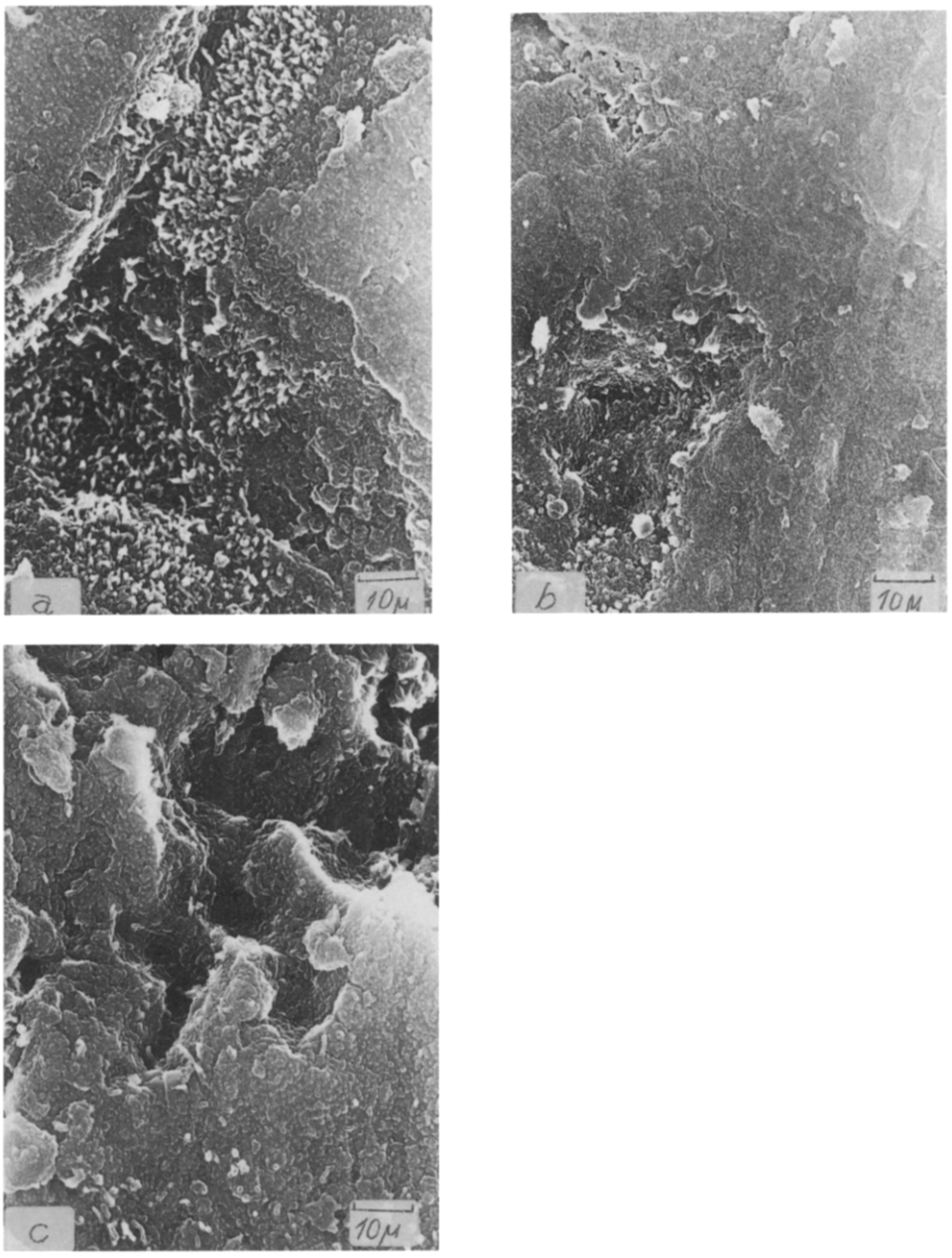

Fig. 4. SEM pictures of Li–Al electrodes (×1000): (a) 0% Mn; (b) 1% Mn, and (c) 2.6% Mn.

pictures exhibit some typical pits and cracks, which are the largest with the samples with 2.6% Mn and the smallest with those with 1.0% Mn. The internal microstructure of the anodes can be seen into the pits at the highest magnifications applied, in Fig. 5. Here we can discern dense agglomerates consisting of spherical crystal grains with

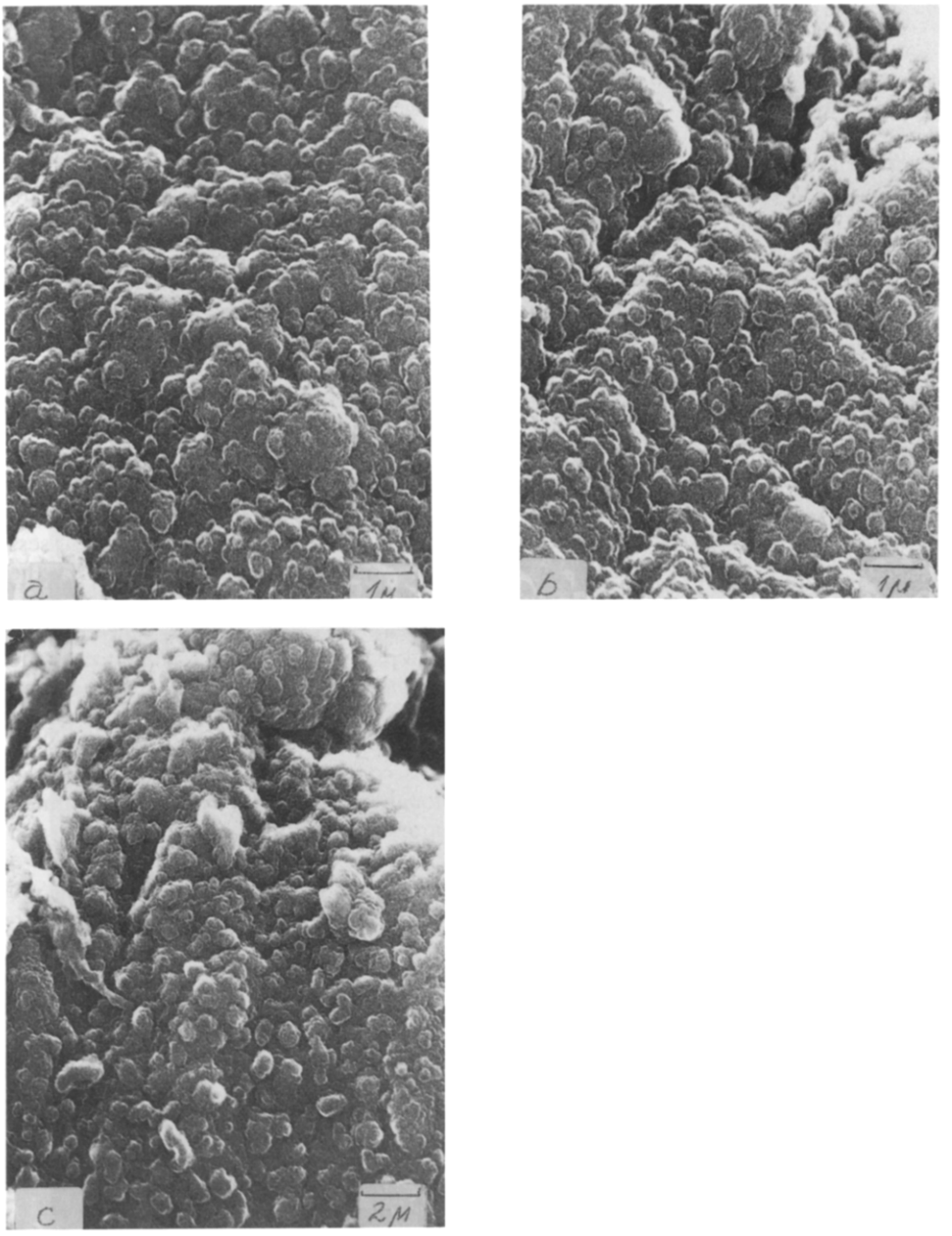

Fig. 5. SEM pictures of Li–Al electrodes: (a) 0% Mn, ×10 000; (b) 1.0% Mn, ×10 000, and (c) 2.6% Mn, ×5000.

a diameter from ~0.2 to 2 μm with smeared edges. Each agglomerate provides a strong framework with tight mechanical and electronic contacts between the grains. As suggested by the considerable hardness of the alloy, the bonds between the agglomerates are also rather strong.

From these pictures, it can be inferred that the presence of 1.0% Mn in the form of solid solution in the Al matrix has a slight but positive effect on the homogeneity of the β-phase layer which is characterized by less numerous and smaller cracks and pits as compared with the two-phase Al matrix with 2.6% Mn. This explains the lower mechanical integrity and the brittleness of the Li–Al anodes with a high Mn content observed by their handling, especially after the end of the cycling test.

The SEM pictures of an electrochemically prepared Li–Al anode without Mn are shown in Fig. 6 for comparison. They reveal a more porous and more densely cracked surface with crystal grains which are less tightly attached to the agglomerates.

A series of measurements of the Li chemical diffusion coefficient D in the β-phase anodes, prepared by the present compression method, were carried out. Data in refs. 13 and 14 claim that the introduction of some transition metals in the crystal lattice of the Al matrix, e.g., Cr, Mn and Ni has a negative effect on the diffusion of Li. On the other hand, Kishio and Brittain [12] have established that the diffusion coefficient of Li in the β phase at 415 °C decreases with the increase in the Li concentration in this phase. The fast diffusion of Li in the β phase is assigned to its defect structure, containing Li vacancies in the Li sublattice. With the increase in the Li concentration in the β-phase range the content of Li vacancies diminishes and consequently the diffusion rate of Li is reduced. Hence, it was of interest to assess which of these two factors has a predominant impact on the value of D in the concentration ranges of Li and Mn in the anodes under investigation.

The experimental D values are plotted in Fig. 7 versus the atomic concentration of Li in the Li–Al anodes. The plot clearly demonstrates the strong influence of the Li concentration on the D value and the negligible effect of Mn at Li concentration above 50 a/o. At lower Li concents, however, the presence of Mn brings about a noticeable decrease in D.

Our experimental value of D at 50 a/o Li is compared with previously reported data of D values in Table 1. The differences, though not very large are to be attributed to the different methods of the anode preparation, methods of measurement and effective surface area.

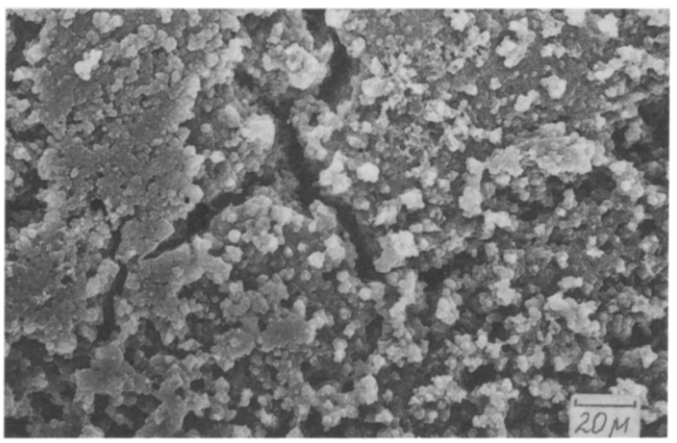

Fig. 6. SEM pictures of electrochemically prepared Li–Al, Mn-free electrode; ×500.

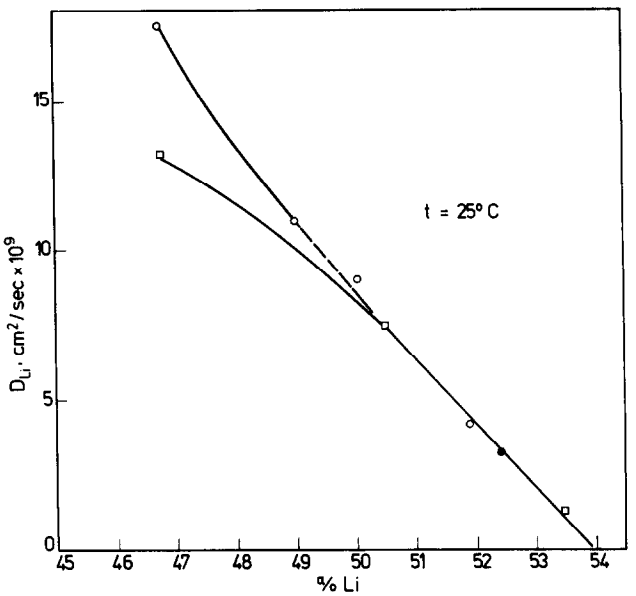

Fig. 7. Chemical diffusion coefficient of Li in Li–Al electrodes at 25 °C as a function of Li concentration: (○) Mn-free; (□) 1% Mn, and (●) 2.6% Mn.

TABLE 1

Diffusion coefficient of Li in β-Li–Al

Author	Year	Reference	Type of sample[a]	Method of measurement[b]	D (cm^2/s)
Willhite	1976	[14]	m.f.	NMR	1.1×10^{-9}
Jow	1982	[5]	p.m.p.	GP	6.4×10^{-9}
Gareau	1983	[15]	e.d.	GP, PP	5.0×10^{-9}
Huang	1990	[16]	p.m.p.	GP	1.4×10^{-9}
Kumagai	1992	[9]	e.d.	PP, AC	$1.7–6.3\times10^{-10}$
This work			p.f.	GP	8.0×10^{-9}

[a]m.f.: metallurgical foil of Li–Al; p.m.p.: pressed metallurgical powder of Li–Al; e.d.: electrochemical deposition; p.f.: pressed foils of Li and Al.
[b]NMR: nuclear magnetic resonance; GP: galvanostatic polarization; PP: potentiostatic polarization; AC: a.c. impedance.

Part 2. Cycling performance of the Li–Al anodes

Experimental

A series of Li–Al anodes were prepared by the above-described method at 70 °C under a pressure of ~1.5 tons/cm^2 for 48 h. The anodes were cycled in laboratory stainless-steel cells provided with a Li/Li^+ reference electrode. The cells simulate completely the conditions in commercial 2016 coin cells, i.e., close packing with a limited electrolyte volume. The electrodes, 15 mm in diameter were separated by one sheet of polypropylene non-woven fabric (0.12 mm). The cathode active material was

$Li_{0.3}MnO_2$ synthesized from $MnCO_3$ and $LiNO_3$ by a method developed in this laboratory. The cathodes were prepared by pressing a mixture of the active material with 20% teflonized acetylene black (TAB 2) on an Al foil. The electrolyte was 1 M $LiClO_4$ in a mixture of PC and DME (1:1). The cells were cycled at room temperature between 1.9 and 3.3 V corresponding to 100% DOD with respect to the cathode, at constant charge and discharge current densities of 1.1 mA/cm^2. Since the cell capacity was cathode limited, the DOD of the anode was varied by changing the cathode mass. The cycling efficiency of the cathode (>99.9%) is much larger than that of the anode (94–96%) and the cell cycling capability is determined by the anode behaviour. The cycling test was terminated when the anode discharge capacity fell down to 70% of the initial one, this determining the number of efficient cycles. As initial discharge capacity, we accept here the one of the fifth cycle, after which the rate of the capacity decay becomes rather stable.

Results and discussion

Figure 8 presents a set of typical discharge/charge curves of a cell at the 5th and the 80th cycle at 22% DOD with an anode containing 1.0% Mn. Similar curves were obtained with cells having anodes without or with 2.6% Mn. It was established by numerous experiments that the cycling behaviour of the anodes with 1.0 and 2.6% Mn differs insignificantly. This is evidenced by the curves in Fig. 9 showing the decay of the specific mass capacity of the three types of Li–Al anodes with the number of cycles. The beneficial effect of Mn on cycling stability is obvious. The only substantial difference found after the cycling test was the considerably higher brittleness of the material with 2.6% Mn, so that the latter appears less suitable for anodes in rechargeable cells. Therefore, in the discussion to follow, we will present mainly the data of the anodes with 1.0% Mn.

Figures 10 and 11 demonstrate the evolution of the anode potential versus Li reference electrode, E, during a single cycle, as well as, the alteration of the E–τ curves with the progress of cycling for two anodes: without Mn and with 1.0% Mn. Despite the small amount of the Mn added, the potential–time curves of these anodes differ considerably from the Mn-free anodes in several respects: first their potential at the end of discharge $(E^d)_{end}$ is higher, second, their average discharge/charge overpotential, η^* is also higher and third, they exhibit two minima in the E–τ charge curves.

The average discharge/charge mid-overpotential, η^*, is introduced here for convenience and it is defined as:

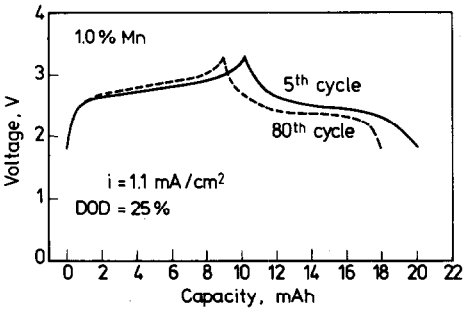

Fig. 8. Charge/discharge curves of a LiAl/Li_yMnO_2 cell at the 5th and 80th cycle, with a Li–Al anode containing 1.0% Mn at 25% DOD.

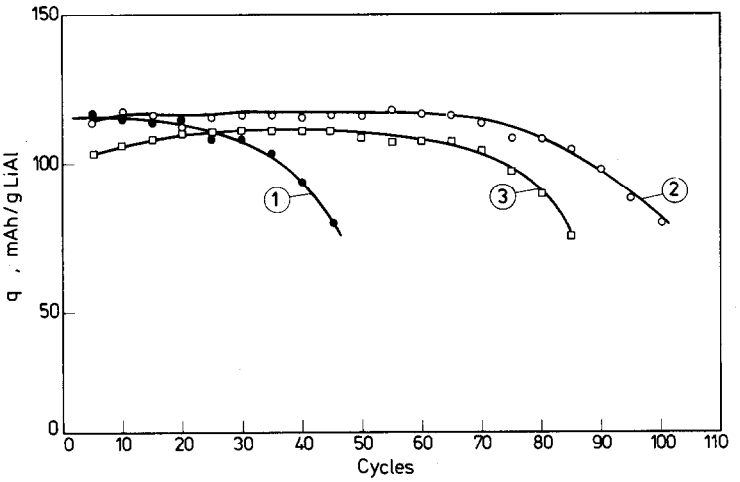

Fig. 9. Decay of the specific mass capacity of Li–Al anodes with the number of cycles: (1) Mn-free anode; (2) anode with 1.0% Mn, and (3) anode with 2.6% Mn.

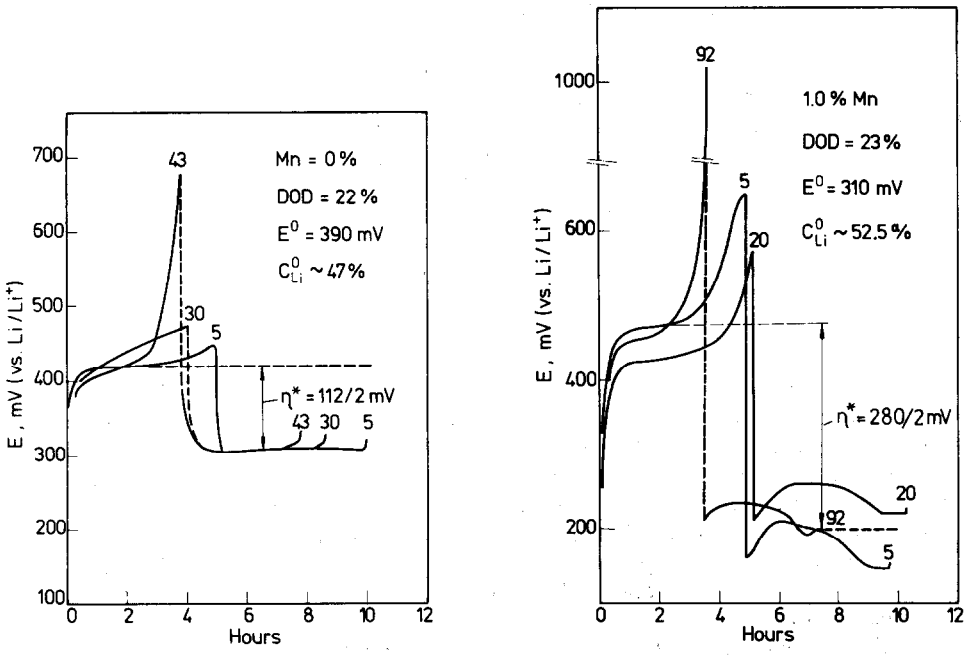

Fig. 10. Potential of the Li–Al Mn-free electrode during charge and discharge at various cycles shown on the curves.

Fig. 11. Potential of the Li–Al electrode with 1.0% Mn during charge and discharge at various cycles shown on the curves.

$$\eta^* = \frac{\eta^d + \eta^c}{2} = \frac{E^d - E^c}{2} \quad (2)$$

where η^d, η^c are the overpotentials of the anode at mid-discharge and mid-charge, respectively, and E^d and E^c are the potentials of the anode versus Li/Li^+ reference electrode at mid-discharge and mid-charge, respectively.

To elucidate the reason for these differences it is necessary to remind that, as shown by curve 3 in Fig. 1 and curve 2 in Fig. 2, the presence of Mn retards the alloying reaction, so that for the time of the preparation of the anodes (48 h) the Li content in the β layer of the Mn-free anodes is lower than that of the Mn-containing anodes. Hence, according to the relationship in Fig. 7, the Li diffusion coefficient of the Mn-free anodes will be higher. This explains the comparatively flat discharge and charge $E-\tau$ curves shown in Fig. 10, as well as the lower η^* and $(E^d)_{end}$ values for the Mn-free alloys.

At the end of discharge of the Mn-containing anode (Fig. 11) the anode surface is more deeply depleted of Li in virtue of its lower Li diffusion coefficient. From the high $(E^d)_{end}$ values of this anode it can be inferred that the surface anode layer contains certain amounts of the α phase. Hence, at the beginning of the next charging, the nucleation of the β-phase on the α-phase grains will require an additional overpotential expressed by the first minimum of the charging part of the $E-\tau$ curve (Fig. 11). At the end of the charging of this anode its surface Li concentration will increase faster than that of the Mn-free anode, because of its lower Li diffusion coefficient. The accumulation of Li at the surface will further decrease the D value and a diffusion overpotential will appear, revealed by the second minimum in the charging $E-\tau$ curve (Fig. 11).

Figure 12 presents the evolution of η^* with the number of cycles, while Fig. 13 shows the evolution of $(E^d)_{end}$ with the number of cycles for three types of anodes. It is seen that the Mn-free anode shows considerably lower η^* and $(E^d)_{end}$ values throughout the cycling test. Nevertheless, the cycle life of this anode is much shorter than those of the Mn-containing anodes. Hence, neither η^* nor $(E^d)_{end}$ values can be regarded as a criterion for the cycling efficiency of the Li–Al anodes.

The cycling performance of the anode cannot be satisfactorily described by the number of efficient cycles attained. The much better criterion in this respect is the cycling efficiency, C_{eff}, defined by:

$$1 - C_{eff} = Q_{ex}/Q_{ac} \quad (3)$$

where Q_{ex} is the excess anode capacity determined from its Li content and Q_{ac} is the total discharge capacity accumulated during the cycling test. It was found that depending on the DOD, the value of C_{eff} varies from 94.4 to 95.5%.

For practical purposes the value $DRF = 1 - C_{eff}$, which is called here arbitrarily degeneration-rate factor, seems more useful since the experimental results show that it is a linear function of DOD (Fig. 14). The effect of DOD on the *DRF* value of the Mn-containing anodes prepared by the present compression method is rather slight. The considerable beneficial effect of Mn, in the range 1.0–2.6%, on the cycling performance is apparent by comparing the *DRF* values of the anodes with and without Mn. This beneficial effect has been previously demonstrated in the case of anodes prepared by pressing of the pyrometallurgical Li–Al powder [16, 17]. The effect of the Mn addition is assigned to the improvement in the mechanical properties of the β-Li–Al layer, as exhibited by its increased hardness. It is supposed that Mn, when present as a solid solution and also as a second phase in minor amounts, retards the

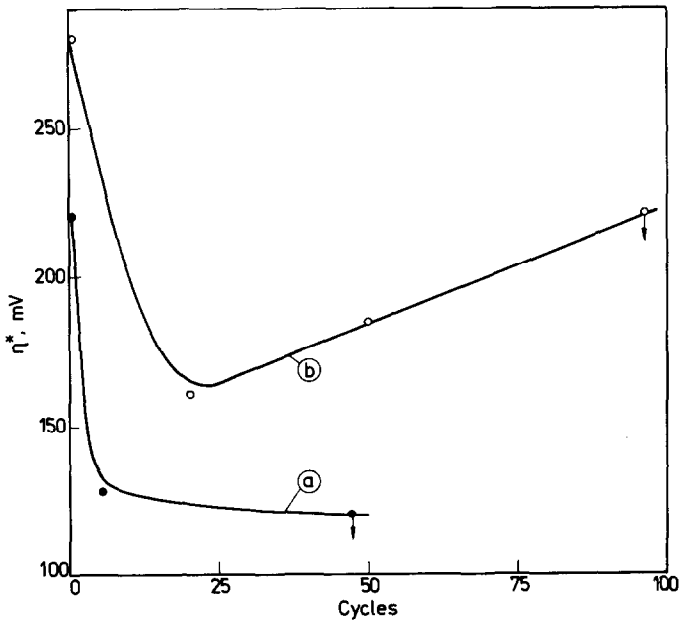

Fig. 12. Average discharge/charge mid-overpotential η^* of Li–Al electrodes as a function of the number of cycles: (a) Mn-free electrode, and (b) electrode with 1.0% Mn.

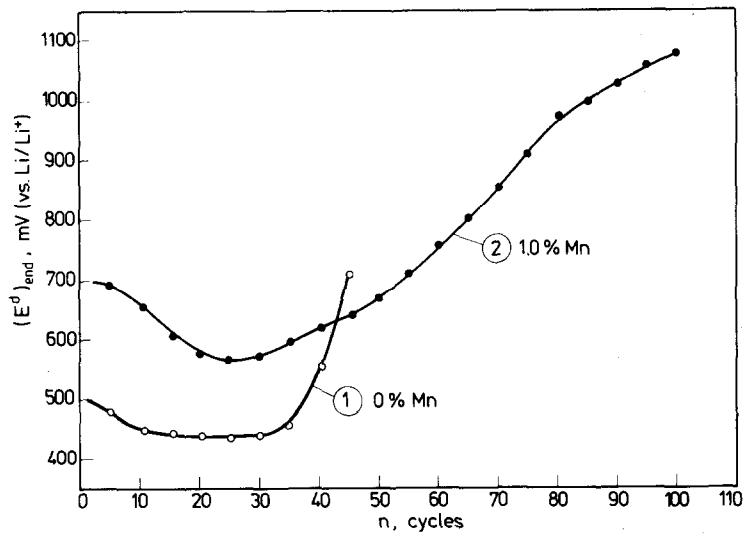

Fig. 13. Anode potential of the end of the discharge $(E^d)_{end}$ as a function of the number of cycles: (1) Mn-free anode, and (2) anode with 1.0% Mn.

propagation of cracks in the crystal grains of the β phase, subjected to the stress caused by the volume variations during cycling, this leading ultimately to the grain disintegration and capacity loss.

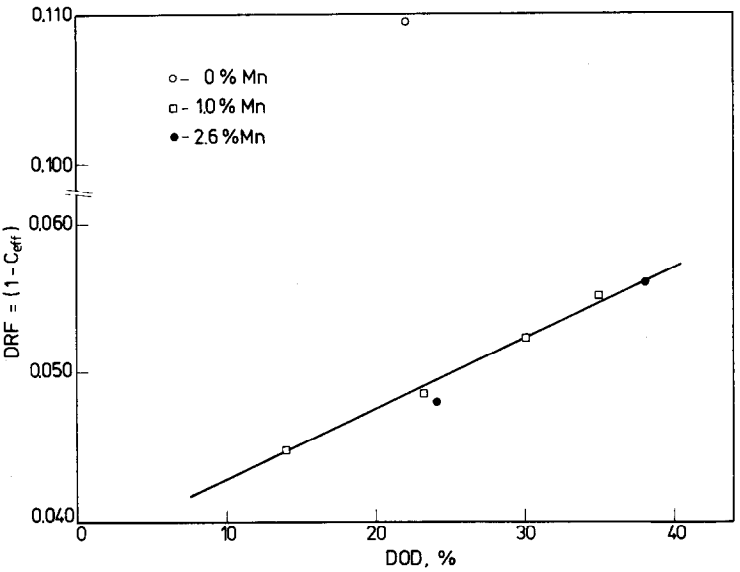

Fig. 14. Effect of DOD on the degradation-rate factor $DRF=(1-C_{eff})$ of Li–Al electrodes: (○) Mn-free; (□) 1.0% Mn, and (●) 2.6% Mn.

Conclusions

The present compression method for the preparation of Li–Al anodes is comparatively simple and proceeds under milder conditions. The porosity of the β-Li–Al layer is limited below 12%, this enhancing its mechanical and, consequently, cycling stability. The addition of 1.0% Mn to the Al substrate improves considerably the resistance of the β-phase crystallites against cracking, whereby the cycling efficiency of the anodes is increased up to 94% at DOD values ranging from 14 to 38%.

Acknowledgements

The authors are indebted to Dr N. Stoichev and Dr V. Michnev for the preparation and the metallographic characterization of the Al and Al–Mn foils used for the anodes. The work was supported financially in part by the National Research Foundation of Bulgaria under contract Ch 60/1993.

List of symbols

D	chemical diffusion coefficient, cm^2/s
L	diffusion length, cm
V_m	molar volume, cm^3/mol
E	potential, mV
E^o	open-circuit potential, mV
E^c	mid-potential at charge, mV
E^d	mid-potential at discharge, mV

$(E^d)_{end}$	potential at the end of discharge, mV
C_{eff}	cycling efficiency, %
Q_{ex}	excess anode capacity, Ah
Q_{ac}	accumulated anode capacity, Ah
$DRF = 1 - C_{eff}$	degeneration-rate factor
q	specific capacity, mAh/g
DOD	depth-of-discharge
η^c	overpotential of the anode at mid-charge, mV
η^d	overpotential of the anode at mid-discharge, mV

References

1 N. Furukawa and T. Nohma, *Ext. Abstr. 6th Int. Meet. Lithium Batteries, Münster, Germany, May 10–15, 1992,* p. 97.
2 J.O. Besenhardt and G. Eichinger, *J. Electroanal. Chem., 68* (1976) 1.
3 M. Epelboin, M. Froment and M. Garreau, *J. Electrochem. Soc., 127* (1980) 2100.
4 A.S. Baranski and W.R. Fawcett, *J. Electrochem. Soc., 129* (1982) 911.
5 T.R. Jow and C.C. Liang, *J. Electrochem. Soc., 129* (1982) 1429.
6 J. Geronov, P. Zlatilova and R. Moshtev, *J. Power Sources, 12* (1984) 145.
7 A.S. Baranski, W.R. Fawcett, T. Krogulec and M. Drogovska, *J. Electrochem. Soc., 131* (1984) 1750.
8 B.M. Rao, R.W. Francis and H.A. Christopher, *J. Electrochem. Soc., 124* (1977) 1490.
9 N. Kumagai, Y. Kikuchi, K. Tanno, F. Lantelme and M. Chemla, *J. Appl. Electrochem., 22* (1992) 728.
10 *Can. Patent No. 1 042 503* (1978).
11 *US Patent No. 4 865 932* (1989).
12 K. Kishio and J.O. Brittain, *J. Phys. Chem. Solids, 40* (1979) 933.
13 I. Hauke, S. Machill, D. Rahner and K. Wiesener, *J. Power Sources, 44* (1993) 21.
14 J.R. Willhite, *J. Phys. Chem. Solids, 37* (1976) 1073.
15 M. Garreau, *J. Power Sources, 9* (1983) 235.
16 C.K. Huang, S. Subbarao, D.H. Shen, F. Deligiannis, A. Attia and G. Halpert, *Proc. Electrochemical Society Symp., Seattle, WA, USA, Oct. 1990,* p. 395.
17 *US Patent No. 4 002 492* (1977).